Electron Spin Resonance Spectra of Reduced $[Fe_2S_2(SC_6H_4Y\text{-}p)_4]^{2-}$ (Y = Cl, H, or Me) Complexes and their Selenium-ligated Homologues

Peter Beardwood and John F. Gibson *
Department of Chemistry, Imperial College of Science and Technology, London SW7 2AY

E.s.r. spectra are reported for the chemically reduced forms of the dimers $[Fe_2S_2(SC_6H_4Y\text{-}p)_4]^{2-}$ (Y = Cl, H, or Me) in *NN*-dimethylformamide (dmf) and 1-methylpyrrolidin-2-one solvents. Where the frozen solvents are non-vitreous, signals having *g* extrema at *ca.* 2.001—2.002, 1.952—1.958, and 1.911—1.915 are observed, which are compatible with those of the $[2Fe\text{–}2S]^+$ ferredoxins and are assigned to the trianions $[Fe_2S_2(SC_6H_4Y\text{-}p)_4]^{3-}$. When the frozen solvents are vitreous, significantly different, solvent-dependent signals are obtained which are indicative of some chemical modification of the complex. The chelated complex trianions $[Fe_2S_2\{(SCH_2)_2C_6H_4\text{-}o\}_2]^{3-}$ and $[Fe_2S_2(btpo)_2]^{3-}$ [btpo = 2,2'-bis(thiophenolate)] give e.s.r. spectra devoid of such solvent dependency, but like the reduced $[Fe_2S_2(SC_6H_4Y\text{-}p)_4]^{2-}$ complexes show a related change in spectrum in the presence of excess Bu^{t}SH. E.s.r. spectra are described for the reduction products of the selenium-bridged complexes $[Fe_2Se_2\{(SCH_2)_2C_6H_4\text{-}o\}_2]^{2-}$, $[Fe_2Se_2(SC_6H_4Y\text{-}p)_4]^{2-}$ (Y = H and Me), and $[Fe_2Se_2(btpo)_2]^{2-}$ and are compared with $[2Fe\text{–}2Se]^+$ ferredoxin spectra. Spectra for reduced $[Fe_2X_2(SePh)_4]^{2-}$ (X = S or Se) are also reported. The broadening of the low-field peaks in the spectra for $[Fe_2S_2(SC_6H_4Cl\text{-}p)_4]^{3-}$ and $[Fe_2Se_2\{(SCH_2)_2C_6H_4\text{-}o\}_2]^{3-}$ in dmf is analysed in the range *ca.* 90—200 K as a convolution product of a fixed Gaussian function with a Lorentzian curve of variable width. The latter is related to a variation in spin-lattice relaxation time with temperature which may be interpreted in terms of an Orbach mechanism involving the first excited state of the spin manifold due to antiferromagnetic coupling of the two iron atoms, such that $-J = 240 \pm 25$ cm^{-1} for $[Fe_2S_2(SC_6H_4Cl\text{-}p)_4]^{3-}$ and $-J = 200 \pm 10$ cm^{-1} for $[Fe_2Se_2\{(SCH_2)_2C_6H_4\text{-}o\}_2]^{3-}$.

The binuclear sulphido-bridged dianions $[Fe_2S_2\{(SCH_2)_2C_6H_4\text{-}o\}_2]^{2-}$ (I) and $[Fe_2S_2(SC_6H_4Y\text{-}p)_4]^{2-}$ (II) (Y = Cl, H, or Me) are exact analogues of the immediate co-ordination environment in $[2Fe\text{–}2S]^{2+}$ ferredoxin centres and display many coincident physical and chemical properties.[1-5] Spectroscopic observations of the trianion $[Fe_2S_2\{(SCH_2)_2C_6H_4\text{-}o\}_2]^{3-}$,

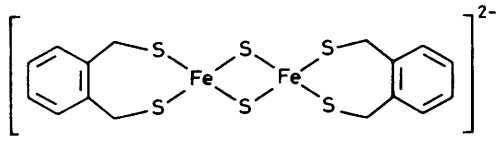

(I)

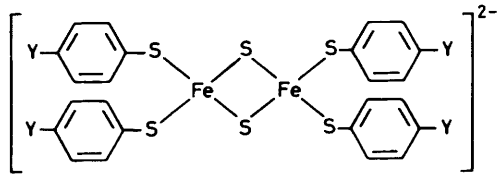

(II)

subsequent to chemical reduction of the corresponding dianion in solution, have recently been reported by Holm and co-workers [6] and by ourselves,[7] but no salts could be isolated. The e.s.r.[6,7] and Mössbauer [7] spectra for this analogue of the $[2Fe\text{–}2S]^+$ ferredoxin centre are characteristically typical of corresponding spectra for these proteins.

For the $[Fe_2S_2(SC_6H_4Y\text{-}p)_4]^{2-}$ complexes, containing unidentate arenethiolate ligands, one-electron reduction can be demonstrated polarographically,[2] but prolonged electrochemical reduction in an attempt to attain bulk concentrations of the trianion leads only to the tetramers $[Fe_4S_4(SC_6H_4Y\text{-}p)_4]^{2-/3-}$ due to facile and irreversible dimerisation.[8]

Chemical, as opposed to electrochemical reduction, however, may be undertaken more rapidly and the reduction products stabilised by immobilisation on freezing the solvent. We report here e.s.r. spectra obtained following reductions of the $[Fe_2S_2(SC_6H_4Y\text{-}p)_4]^{2-}$ (Y = Cl, H, or Me) complexes in various solvents, together with spectra for $[Fe_2Se_2\{(SCH_2)_2C_6H_4\text{-}o\}_2]^{3-}$ and for the products following reduction of $[Fe_2X_2(XPh)_4]^{2-}$ (X = S or Se). Preliminary e.s.r. data for reduction of the new complex $[Fe_2S_2(btpo)_2]^{2-}$ [btpo = 2,2'-bis(thiophenolate)] in various solvents are also described. We report temperature-dependent spin-lattice relaxation measurements from lineshape analyses for $[Fe_2Se_2\{(SCH_2)_2C_6H_4\text{-}o\}_2]^{3-}$ and $[Fe_2S_2(SC_6H_4Cl\text{-}p)_4]^{3-}$ in their regions of spectral broadening.

Experimental

Preparative.—All preparative procedures were carried out under purified dinitrogen or argon atmospheres using deoxygenated solvents. The solvents mpo (1-methylpyrrolidin-2-one), dmf (*NN*-dimethylformamide), and PhCN were carefully dried and distilled prior to use. $[NEt_4]_2[Fe_2S_2\{(SCH_2)_2C_6H_4\text{-}o\}_2]$ was prepared from $[NEt_4][Fe\{(SCH_2)_2C_6H_4\text{-}o\}_2]$ [9] by reaction with sodium hydrogensulphide in methanol.[8] $[NEt_4]_2[Fe_2Se_2\{(SCH_2)_2C_6H_4\text{-}o\}_2]$ [4] was made in a similar way using sodium hydrogenselenide.[10]

$[NEt_4]_2[Fe_2X_2(SC_6H_4Y\text{-}p)_4]$ (X = S or Se; Y = H, Me, or Cl) were synthesised by ligand substitution from $[NEt_4]_2[Fe_2X_2\{(SCH_2)_2C_6H_4\text{-}o\}_2]$ in acetonitrile.[2] Previously unreported $[NEt_4]_2[Fe_2X_2(SePh)_4]$ (X = S or Se) were prepared in a similar manner to the PhS-ligated complexes by the following method.

To a stirred slurry of $[NEt_4]_2[Fe_2X_2\{(SCH_2)_2C_6H_4\text{-}o\}_2]$ (1.5 mmol) in acetonitrile (50 cm^3) was added a solution of PhSeSePh (30 mmol) [11] in acetonitrile (200 cm^3). After about 15 min the reaction mixture developed a dark purple-black colouration and was stirred overnight. Reduction of the solvent volume to around 150 cm^3 resulted in separation of excess

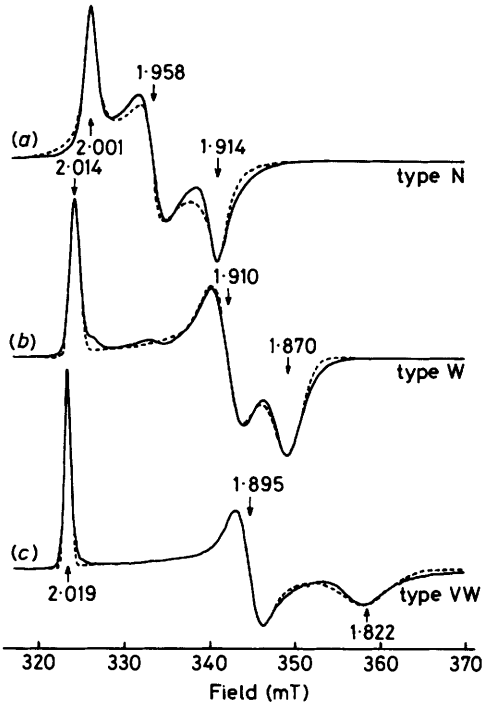

Figure 1. E.s.r. spectra for reduced $[Fe_2S_2(SC_6H_4Y\text{-}p)_4]^{2-}$ at *ca.* 100 K (——) together with simulations (– – –). (*a*) Y = Cl in non-vitreous dmf (microwave power, field modulation amplitude, microwave frequency: 20 mW, 0.4 mT, 9.145 GHz). (*b*) Y = H in vitreous 0.1 mol dm^{-3} $[NBu^n_4][ClO_4]$–dmf (20 mW, 0.2 mT, 9.143 GHz). (*c*) Y = Me in vitreous 0.2 mol dm^{-3} $[NBu^n_4][ClO_4]$–mpo (8 mW, 0.25 mT, 9.141 GHz). The *g* values marked with arrows refer to the simulations, data for which are collected in Table 1

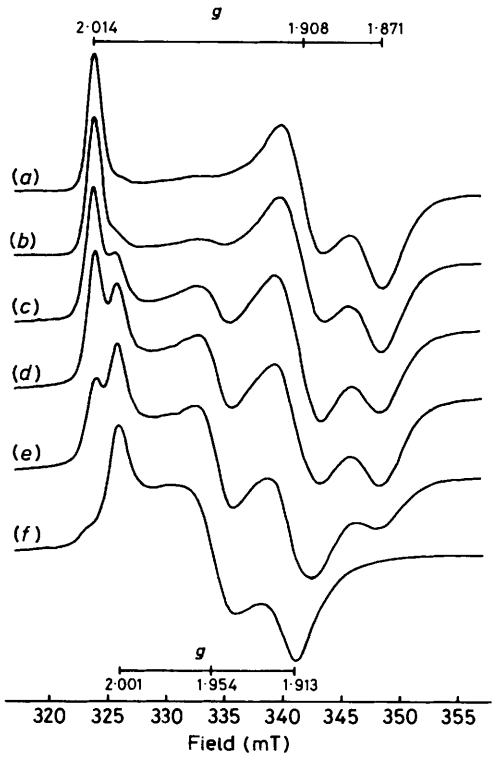

Figure 2. E.s.r. spectra for $[Fe_2S_2(SPh)_4]^{2-}$ reduced in dmf containing (*a*) 17, (*b*) 9, (*c*) 4, (*d*) 2, (*e*) 1, and (*f*) 0% (v/v) CH_2Cl_2. The spectra are individually normalised to have the same height (microwave power 20 mW, field modulation amplitude 0.32 mT, microwave frequency 9.13 GHz, *T ca.* 100 K)

ligand and after filtration the crude product was precipitated with tetrahydrofuran (thf) (200 cm^3). The solid was separated by filtration from a grey-brown filtrate, spectral examination of which revealed the presence of a substantial proportion of $[Fe_4X_4(SePh)_4]^{2-}$.[12] The black solid was recrystallised from acetonitrile–thf to give 40% (X = S) or 25% (X = Se) yields of purple-black crystals {Found: C, 45.1; H, 5.65; N, 2.8. Calc. for $[NEt_4]_2[Fe_2S_2(SePh)_4]$ C, 45.45; H, 5.7; N, 2.65%. Found: C, 41.85; H, 5.3; N, 2.4. Calc. for $[NEt_4]_2[Fe_2Se_2(SePh)_4]$: C, 41.6; H, 5.25; N, 2.45%}. Visible spectrum in dmf, λ/nm (10^{-3} ε/dm^3 mol^{-1} cm^{-1}): $[Fe_2S_2(SePh)_4]^{2-}$, 353 (18.8), 500 (sh), 552 (11.6); $[Fe_2Se_2(SePh)_4]^{2-}$, 355 (16.7), 540 (10.4).

The more soluble $[NBu^n_4]^+$ salt of $[Fe_2S_2\{(SCH_2)_2C_6H_4\text{-}o\}_2]^{2-}$ [6] was used for reduction in mpo. $[NBu^n_4]_2[Fe_2X_2(btpo)_2]$ (X = S or Se) were prepared in a similar manner using the ligand 2,2′-bis(thiophenol).[13] Visible spectrum in acetonitrile λ/nm (10^{-3} ε/dm^3 mol^{-1} cm^{-1}): $[Fe_2S_2(btpo)_2]^{2-}$ 335 (21.8), 375 (sh), 425 (19.1), 460 (sh), 518 (9.1), 550 (sh) (8.5); $[Fe_2Se_2(btpo)_2]^{2-}$ 343 (22.7), 382 (sh) (17.8), 456 (16.9), 500 (sh), 588 (6.8), ~650 br (sh).

Reductions were performed in the manner previously described [7] using monosodium acenaphthylenide generated in dmf or mpo solution from acenaphthylene reduced over 0.1—0.2% sodium–mercury amalgam.

E.S.R. Measurements.—E.S.R. spectra were recorded using a Varian E12 spectrometer operating at *ca.* 9.2 GHz and, unless otherwise stated, at a temperature of *ca.* 100 K. Samples were cooled in a stream of nitrogen gas the temperature of which was regulated by a Varian variable-temperature accessory. For the spectra used in determining spin-lattice relaxation values the sample temperature was measured with a copper–constantan thermocouple located in the gas stream just above the sample. For measurements at 77 K the sample was immersed in liquid nitrogen in a finger-dewar inside the cavity. Spectra were recorded digitally using 1 000 data points. Anisotropic e.s.r. spectral simulations were performed by spatial integration as previously described [7] and were least-squares fitted to the experimental lineshape.

Reduction of the Dianionic Dimer Complexes.—Reduction in pure solvents, non-vitreous when frozen. The e.s.r. signal obtained on reducing $[Fe_2S_2(SC_6H_4Cl\text{-}p)_4]^{2-}$ in dmf is shown in Figure 1(*a*) and has *g* extrema at 2.002, 1.958, and 1.915 (except where specified, the *g* values given throughout this paper are those measured directly from the maximum, crossover, and minimum of the first-derivative experimental spectrum). Reduction of $[Fe_2S_2(SC_6H_4Y\text{-}p)_4]^{2-}$ (Y = H or Me) in dmf leads to signals with comparable *g* values to these (2.001—2.002, 1.954, and 1.913—1.914) but having somewhat larger linewidths. All three complexes when reduced in mpo or PhCN give rise to signals having *g* values closely similar to those obtained where dmf is used as solvent, and we label this signal type N (narrow anisotropy). *g* Values for the various signals described and their simulations are collected in Table 1.

Reduction in solvents frozen as glasses. None of the above solvents produces a glassy matrix on freezing but rather the solvent attains a high degree of crystallinity. If, however, the dmf or mpo contains, for example, 0.1—0.2 mol dm^{-3} $[NBu^n_4][ClO_4]$ or *ca.* 20% (v/v) dichloromethane, then a transparent glass is produced when the mixture is rapidly

cooled in liquid nitrogen. Reduction of the three complexes $[Fe_2S_2(SC_6H_4Y\text{-}p)_4]^{2-}$ (Y = Cl, H, or Me) in these solvent systems produces very different e.s.r. spectra from those obtained in the pure solvents. $[Fe_2S_2(SPh)_4]^{2-}$ reduced in 0.1 mol dm^{-3} $[NBu^n_4][ClO_4]$–dmf gives an e.s.r. spectrum having g extrema at 2.014, 1.910, and 1.871 [Figure 1(*b*)]. A small residual component similar to the narrower type N signal obtained with the pure solvent may be seen between the features at 2.014 and 1.910. The same complex reduced in dmf containing concentrations of CH_2Cl_2 in the range 0—2 mol dm^{-3} shows a steady change, as the sample becomes increasingly glassy, from the type N signal having g extrema at 2.001, 1.954, and 1.913 to a signal characterised by the turning points g = 2.014, 1.908, and 1.871 (Figure 2). The latter signal obtained from the vitreous sample is much the same as that shown in Figure 1(*b*) where the solvent contained 0.1 mol dm^{-3} $[NBu^n_4][ClO_4]$. We label this type of signal as type W (wide anisotropy). Other additives such as water, toluene, or methanol can also result in the solvent freezing in a glassy state; such mixtures also give rise to the type W signal in the e.s.r. spectra observed upon reduction of dissolved dimer. The e.s.r. spectrum given by $[Fe_2S_2(SC_6H_4Me\text{-}p)_4]^{2-}$ after reduction in dmf and freezing to a glassy sample has comparable g values (2.016, 1.910, and 1.870) to the type W signal of reduced $[Fe_2S_2(SPh)_4]^{2-}$ and is given the same designation.

Even in pure dmf, reduced $[Fe_2S_2(SPh)_4]^{2-}$ shows a small shoulder at low field corresponding to the type W signal observed in the vitreous state. For $[Fe_2S_2(SC_6H_4Me\text{-}p)_4]^{2-}$ this is more pronounced, such that the type N signal is accompanied by *ca.* 10% of the type W signal. In the case of $[Fe_2S_2(SC_6H_4Cl\text{-}p)_4]^{2-}$ reduced in pure dmf the spectrum is

Table 1. E.s.r. data for $[2Fe\text{–}2S]^+$ centres in reduced $[Fe_2S_2(SR)_4]^{2-}$ complexes and in ferredoxins

Y	Solvent [a]	Conditions and comments	Approximate composition [b] %	rest	g_z	g_y	g_x	Ref. in Figure 8
(*a*) Reduced $[Fe_2S_2(SC_6H_4Y\text{-}p)_4]^{2-}$								
Cl	dmf (nv)		100N		2.002	1.958	1.915	
					2.001 [c]	1.958 [c]	1.914 [c]	g
					0.85 [d]	1.35 [d]	1.3 [d]	
H	dmf (nv)		>95N	W	2.001	1.954	1.913	f
Me	dmf (nv)		90N	W	2.002	1.954	1.914	
Me	dmf (v)	0.1 mol dm^{-3} $[NBu^n_4][ClO_4]$ + ten-fold excess p-MeC_6H_4SH	100N		2.002	1.952	1.917	
Cl	mpo (nv)		95N	VW	2.002	1.957	1.915	
H	mpo (nv)		75N	VW	2.002	1.953	1.913	
Me	mpo (nv)		60N	VW	2.001	1.954	1.914	
Cl	PhCN (nv)		100N		2.001	1.957	1.914	
H	PhCN (nv)		100N		2.001	1.952	1.911	
Me	PhCN (nv)		80N		2.001	1.953	1.911	
Cl	dmf (v)	0.1 mol dm^{-3} $[NBu^n_4][ClO_4]$	30W	N	2.013	—	1.873	
H	dmf (v)	0.1 mol dm^{-3} $[NBu^n_4][ClO_4]$	95W	N	2.014	1.910	1.871	
					2.014 [c]	1.910 [c]	1.870 [c]	m
					0.68 [e]	1.65 [e]	1.85 [e]	
H	dmf (dv)	0.1 mol dm^{-3} $[NBu^n_4][ClO_4]$	95VW	N	2.021	1.901	1.822	r
Me	dmf (v)	0.1 mol dm^{-3} $[NBu^n_4][ClO_4]$	100W		2.016	1.910	1.870	
Me	dmf (dv)	0.1 mol dm^{-3} $[NBu^n_4][ClO_4]$	100VW		2.021	1.897	1.829	o
Cl	mpo (v)	0.2 mol dm^{-3} $[NBu^n_4][ClO_4]$	50VW	N	2.019	*ca.* 1.90	1.817	
H	mpo (v)	0.2 mol dm^{-3} $[NBu^n_4][ClO_4]$	100VW		2.019	1.895	1.820	q
Me	mpo (v)	0.2 mol dm^{-3} $[NBu^n_4][ClO_4]$	100VW		2.020	1.895	1.824	
					2.019 [c]	1.895 [c]	1.822 [c]	p
					0.48 [e]	1.47 [e]	2.90 [e]	
H	dmf (v)	17% CH_2Cl_2	100W		2.014	1.908	1.871	
Me	dmf (v)	17% CH_2Cl_2	100W		2.014	1.909	1.872	
Me	mpo (v)	17% CH_2Cl_2	95W	N	2.019	1.894	1.821	
H	dmf (v)	5% H_2O	100W		2.013	1.911	1.872	
Me	dmf (v)	2% H_2O	100W		2.015	1.913	1.874	
H	dmf (v)	0.1 mol dm^{-3} $[NBu^n_4][ClO_4]$ + 50 times excess Bu^{t}SH	95	N	2.019	1.887	1.845	
H	dmf (v)	0.1 mol dm^{-3} $[NBu^n_4][ClO_4]$ + 50 times excess EtSH	100		2.020	1.894	1.846	
Cl	mpo (v)	0.2 mol dm^{-3} $[NBu^n_4][ClO_4]$ + 50 times excess Bu^{t}SH	100		2.021	1.889	1.843	
Me	mpo (v)	0.2 mol dm^{-3} $[NBu^n_4][ClO_4]$ + 50 times excess Bu^{t}SH	100		2.020	1.890	1.842	n
(*b*) $[Fe_2S_2\{(SCH_2)_2C_6H_4\text{-}o\}_2]^{3-}$								
	dmf (v)	0.1 mol dm^{-3} $[NBu^n_4][ClO_4]$			2.007	1.940	1.922	c
	mpo (v)	0.2 mol dm^{-3} $[NBu^n_4][ClO_4]$			2.009	1.948	1.920	e
	dmf (v)	0.1 mol dm^{-3} $[NBu^n_4][ClO_4]$ + 50 times excess Bu^{t}SH			2.020	1.882	1.846	
					2.020 [c]	1.882 [c]	1.845 [c]	l
					0.43 [e]	1.55 [e]	2.1 [e]	
(*c*) Reduced $[Fe_2S_2(btpo)_2]^{2-}$								
	dmf (v)	0.1 mol dm^{-3} $[NBu^n_4][ClO_4]$, 77 K			2.025	1.914	1.914	a
	mpo (v)	0.2 mol dm^{-3} $[NBu^n_4][ClO_4]$, 77 K			2.024	1.916	1.916	
	mpo (v)	0.2 mol dm^{-3} $[NBu^n_4][ClO_4]$ + 50 times excess Bu^{t}SH			2.020	1.896	1.842	

Table 1 (*continued*)

(*d*) Ferredoxins

	Ref.	g_z	g_y	g_x	Ref. in Figure 8
Adrenodoxin	*f*	2.02	1.935	1.93	(i)
Pseudomonas putida	*f*	2.02	1.935	1.93	(ii)
Clostridium pasteurianum	*g*	2.01	1.95	1.93	(iii)
Azotobacter vinelandii I_A	*h*	2.009	1.941	1.917	(iv)
Azotobacter vinelandii I_B	*h*	2.009	1.943	1.918	(iv)
Azotobacter vinelandii II	*h*	2.035	1.943	*ca.* 1.90	(v)
Parsley	*i*	2.049	1.954	1.897	(vi)
Spinach (powder)	*j*	2.045	1.947	1.881	(vii)
Microcystic flos-acquae	*k*	2.05	1.96	1.89	(viii)
Spinach (solution)	*i*	2.046	1.957	1.886	(ix)
Spirulina maxima	22	2.051	1.958	1.887	(x)
Scenedesmus	22	2.052	1.961	1.887	(xi)
Synechococcus lividus	*l*	2.05	1.96	1.88	(xii)

[a] v = Vitreous, nv = non-vitreous, dv = devitrified. [b] N, W, and VW = spectral types referred to in text; % compositions are estimated from peak heights only. [c] *g* Values from simulation. [d] Lorentzian width (mT) used for simulation. [e] Gaussian width (mT) used for simulation. [f] J. Fritz, R. Anderson, J. Fee, G. Palmer, R. H. Sands, J. C. M. Tsibris, I. C. Gunsalus, W. H. Orme-Johnson, and H. Beinert, *Biochim. Biophys. Acta*, 1971, **253**, 110. [g] W. H. Orme-Johnson and R. H. Sands, in 'Iron–Sulphur Proteins,' ed. W. Lovenberg, Academic Press, New York, 1973, vol. 2, ch. 5. [h] D. V. Devartanian, Y. I. Shethna, and H. Beinert, *Biochim. Biophys. Acta*, 1969, **194**, 548. [i] J. A. Fee and G. Palmer, *Biochim. Biophys. Acta*, 1971, **245**, 175. [j] K. Mukai, T. Kimura, J. Helbert, and L. Kevan, *Biochim. Biophys. Acta*, 1973, **295**, 49. [k] K. K. Rao, R. V. Smith, R. Cammack, M. C. W. Evans, D. O. Hall, and C. E. Johnson, *Biochem. J.*, 1972, **129**, 1159. [l] R. E. Anderson, W. R. Dunham, R. H. Sands, A. J. Bearden, and H. L. Crespi, *Biochim. Biophys. Acta*, 1975, **408**, 306.

very nearly 100% type N, as may be seen from Figure 1(*a*). This same complex when reduced in dmf containing 0.1 mol dm^{-3} $[NBu^n_4][ClO_4]$, to give a glassy sample, shows a spectrum which is a composite of the type N (*ca.* 70%) and type W (*ca.* 30%) signals (the figures of relative composition given in this section are estimates derived from peak heights and are presented to indicate the approximate make-up of the spectra rather than as quantitative integrated intensities). The propensity to produce a type W as opposed to a type N signal is seen to be dependent on the *para* substituent of the arenethiolate ligand in such a way as to increase along the series Y = Cl < H < Me. A similar effect was observed with the reductions performed in mpo.

Figure 1(*c*) shows an e.s.r. spectrum measured for $[Fe_2S_2(SC_6H_4Me\text{-}p)_4]^{2-}$ after reduction in 0.2 mol dm^{-3} $[NBu^n_4][ClO_4]$–mpo, with *g* extrema at 2.020, 1.895, and 1.824. Closely similar spectra were observed for the PhS-ligated dimer and also when mpo–CH_2Cl_2 (5 : 1) was used in place of the quaternary ammonium salt solution. We label such signals type VW (very wide anisotropy). Spectra obtained from samples of dimer enriched in ^{57}Fe showed a splitting of the sharp peak at *g ca.* 2.020 according to that expected for an interaction of the electron spin with two iron nuclei. As stated previously, reduction of any of the three $[Fe_2S_2(SC_6H_4Y\text{-}p)_4]^{2-}$ dimers in pure mpo leads to spectra having a dominant component which closely matches the type N signal observed in dmf; for example, the *g* extrema occur at 2.002, 1.957, and 1.915 for Y = Cl. The secondary component in these spectra is type VW and represents *ca.* 5—10% when Y = Cl, *ca.* 25% for Y = H, and *ca.* 40—50% for Y = Me. This order of decreasing tendency to give the type N signal is in keeping with the series described above. Glassy samples of reduced $[Fe_2S_2(SC_6H_4Cl\text{-}p)_4]^{2-}$ in mpo showed a mixture (*ca.* 1 : 1) of type N and type VW signals, similar to the behaviour in dmf where a mixture of type N and type W was obtained.

Two modes of freezing in glass-forming solvents. Although the solutions containing $[NBu^n_4][ClO_4]$ give a glassy matrix when cooled rapidly in liquid nitrogen, they may be induced to crystallise in two different ways. Thus, for 0.1 mol dm^{-3} $[NBu^n_4][ClO_4]$–dmf, freezing at *ca.* −110 to −120 °C (ethanol slush bath) results in a crystalline mass. Alternatively, if the same solution is rapidly frozen in liquid nitrogen to give a glass, subsequent warming to *ca.* −120 °C causes crystallisation.

For $[Fe_2S_2(SC_6H_4Y\text{-}p)_4]^{2-}$ reduced in 0.2 mol dm^{-3} $[NBu^n_4][ClO_4]$–mpo, crystalline samples may be obtained by freezing at *ca.* −90 °C and, compared with a glassy sample, show an increase in the proportion of N type signal, relative to type VW, which is dependent on Y (Cl > H > Me).

More surprisingly, when the same complexes are reduced in 0.1 mol dm^{-3} $[NBu^n_4][ClO_4]$–dmf and frozen as crystalline samples at −110 °C, a mixture of type N and type VW signals is again observed. As we have seen in the previous section, predominantly type W signals are expected for vitreous samples in dmf solutions, and indeed on thawing the crystalline samples and refreezing as a glass such signals are produced. Alternatively, if a vitreous dmf sample of reduced $[Fe_2S_2(SC_6H_4Me\text{-}p)_4]^{2-}$ having a wholly type W spectrum with *g* extrema at 2.016, 1.910, and 1.870 is warmed to −120 °C, crystallisation takes place and the new signal which is observed is wholly type VW having *g* values of 2.021, 1.897, and 1.829. On thawing and refreezing as a glass this reverts to a wholly type W spectrum. The same change may be observed with the dimer having Y = H but with the additional complication of the presence of some type N signal.

Reduction in the presence of excess ligand. When the reductions of the three complexes in either dmf or mpo were performed in the presence of excess thiol ligand a promotion of the proportion of type N signal in the resulting e.s.r. spectrum was observed. Thus, for reduction of $[Fe_2S_2(SC_6H_4Me\text{-}p)_4]^{2-}$ in 0.1 mol dm^{-3} $[NBu^n_4][ClO_4]$–dmf containing *p*-MeC_6H_4SH at a concentration ten times that of the dimer, a vitreous sample results which has a sharp type N e.s.r. signal (*g* values 2.002, 1.952, and 1.917) in contrast to the type W signal (*g* values 2.016, 1.910, and 1.870) obtained in the absence of thiol. With only a four-fold thiol excess the resulting spectrum is still more than 90% type N. Comparable excesses of $Na(SC_6H_4Y\text{-}p)$ in place of thiol were observed to have little or no effect on the e.s.r. in vitreous samples.

Reduction of $[Fe_2S_2(btpo)_2]^{2-}$. Spectra of $[Fe_2S_2(btpo)_2]^{2-}$ reduced in dmf containing 0.1 mol dm^{-3} $[NBu^n_4][ClO_4]$ are

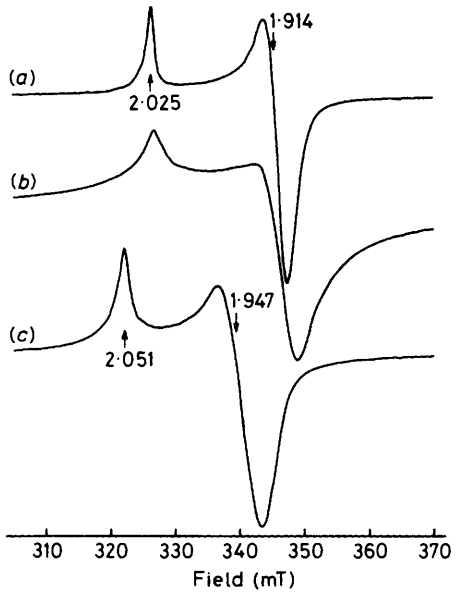

Figure 3. E.s.r. spectra for $[Fe_2X_2(btpo)_2]^{2-}$ (X = S or Se) reduced in dmf containing 0.1 mol dm^{-3} $[NBu^n_4][ClO_4]$ (microwave frequency 9.25 GHz). (*a*) X = S at 77 K (microwave power 8 mW, field modulation amplitude 0.2 mT). (*b*) X = S at 132 K (20 mW, 0.5 mT). (*c*) X = Se at 77 K (8 mW, 0.25 mT)

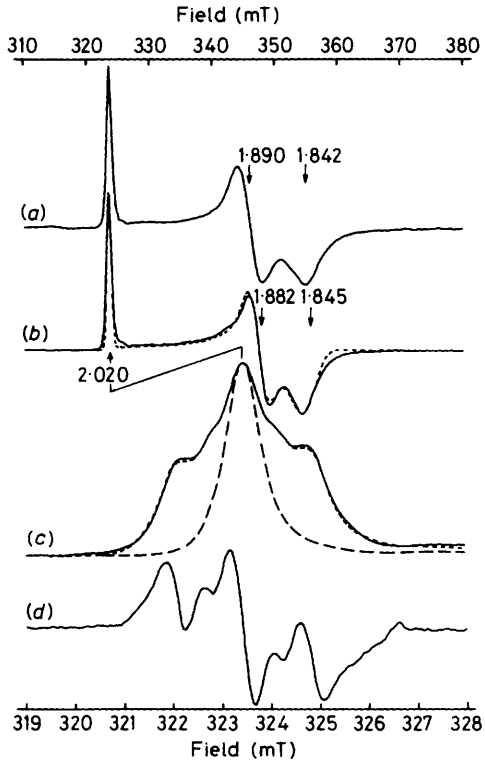

Figure 4. E.s.r. spectra from products of reductions in the presence of a 50-fold excess of Bu^{t}SH. (*a*) Reduced $[Fe_2S_2(SC_6H_4Me\text{-}p)_4]^{2-}$ in 0.2 mol dm^{-3} $[NBu^n_4][ClO_4]$–mpo (microwave power, field modulation amplitude, microwave frequency: 30 mW, 0.4 mT, 9.144 GHz). (*b*) Reduced $[Fe_2S_2\{(SCH_2)_2C_6H_4\text{-}o\}_2]^{2-}$ in 0.1 mol dm^{-3} $[NBu^n_4][ClO_4]$–dmf (12 mW, 0.2 mT, 9.149 GHz); marked *g* values refer to the simulation (– – – –). (*c*) Low-field peak of a spectrum for 83% ^{57}Fe enriched $[Fe_2S_2\{(SCH_2)_2C_6H_4\text{-}o\}_2]^{2-}$ reduced in 0.1 mol dm^{-3} $[NBu^n_4][ClO_4]$–dmf (——) together with a simulation (– – –) constructed from field-shifting the peak observed with naturally occurring Fe (— — —). (*d*) Second-derivative presentation of the ^{57}Fe enriched spectrum in (*c*)

shown in Figure 3(*a*) and (*b*) at temperatures of 77 and 132 K. Closely similar spectra were found using pure dmf or using mpo as solvents, though the vitreous samples gave slightly narrower linewidths. The *g* tensor in these spectra is close to axial ($g_{\|}$ = 2.024—2.025, $g_{\perp}$ = 1.914—1.916). The spectrum is broadened even at 77 K such that its ' wings ' extend for a considerable field spread. Further rapid broadening ensues at higher temperatures [Figure 3(*b*)] and the spectrum is greatly diminished in amplitude and resolution by *ca.* 170 K. At low temperature the low-field peak shows considerable asymmetry in that the extensive tailing to low field is not reflected on the high-field side.

Stability. The reduced unidentate arenethiol-ligated dimers are less stable in mobile solution than is $[Fe_2S_2\{(SCH_2)_2C_6H_4\text{-}o\}_2]^{3-}$. Conversion to the corresponding tetramer, $[Fe_4S_4(SC_6H_4Y\text{-}p)_4]^{2-}$, is readily seen on comparing room-temperature visible absorption spectra before reduction with those taken several minutes after reduction. These spectral results indicate 80—90% dimerisation. No appreciable e.s.r. signals were observed when reductions were performed in the solvents dimethyl sulphoxide (dmso) or acetonitrile.

Yields of the trianionic dimers from reductions of the dianions, as determined by double integration of e.s.r. signals and comparison with Cu^{II} ethylenediaminetetra-acetic acid standards, were dependent on the ligand, the solvent, and on any additives to the solvent system. The yields obtained also varied from one reduction to another due to differences in the time taken to perform the reaction, transfer, and freezing procedures. The highest yields were found for Y = H and Me in mpo (50—60%) but more generally the yields were 20—60%.

Computer simulations. Attempted simulations of the three different spectral types are shown in Figure 1 as overlaid dashed lines. The spectra for vitreous samples were best simulated assuming a Gaussian convolution lineshape. The non-vitreous samples, on the other hand, gave spectra more closely approaching Lorentzian. This may be indicative of spin–spin broadening in the latter samples due to increased magnetic concentration as a consequence of exclusion of the reduced dimer from the solvent crystal lattice. In all the spectra it proved difficult to obtain a good fit around g_x. The spectra for reduced $[Fe_2S_2(btpo)_2]^{2-}$ were rather poorly fitted by the lineshape simulation method employed.

Reductions in the presence of Bu^{t}SH *and* EtSH. During investigation of the effect upon the dimer e.s.r. spectra of adding excess ligand thiol, reductions in the presence of the less protic t-butanethiol and ethanethiol were studied. A completely new solvent-independent signal was observed. Figure 4(*a*) shows a spectrum for $[Fe_2S_2(SC_6H_4Me\text{-}p)_4]^{2-}$ reduced in mpo containing 0.2 mol dm^{-3} $[NBu^n_4][ClO_4]$, to produce a glassy sample, together with Bu^{t}SH at a concentration 50 times that of the dimer. Smaller concentrations of Bu^{t}SH (*ca.* ten-fold excess) also led to this signal, but together with a proportion of the type VW signal. The signal has *g* extrema at 2.020, 1.890, and 1.842 and a particularly sharp B_z peak reminiscent of the type VW signal observed in mpo. The same signal was seen when using dmf as solvent instead of mpo. Closely similar spectra were also found for the Y = H and Y = Cl dimers reduced in the same way, and when using EtSH in place of Bu^{t}SH. If the reduction in the presence of Bu^{t}SH was performed in a solvent containing no glass-forming additive, the resulting spectrum was a mixture of the new signal and the normal type N signal.

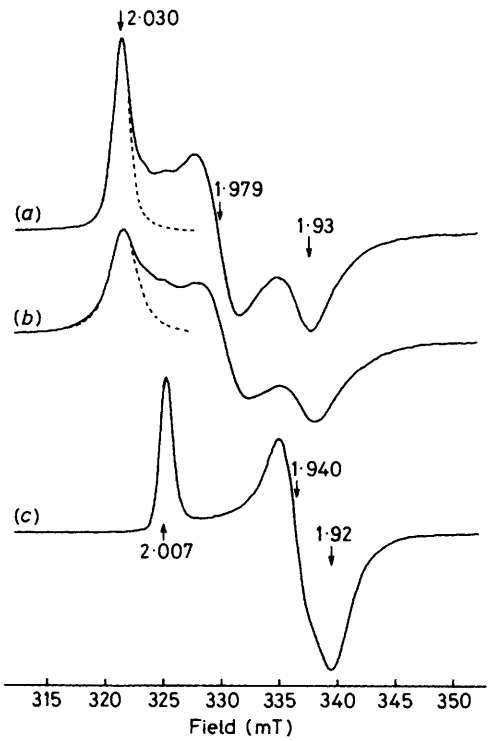

Figure 5. E.s.r. spectra for reduced $[Fe_2X_2\{(SCH_2)_2C_6H_4\text{-}o\}_2]^{2-}$. (*a*) X = Se in dmf at 86 K (microwave power, field modulation amplitude, microwave frequency: 20 mW, 0.25 mT, 9.133 GHz); (– – – –) simulation using $\delta B_L^0 = 0.39$ mT, $\delta B_G^0 = 0.63$ mT. (*b*) X = Se in dmf at 161 K (80 mW, 0.4 mT, 9.133 GHz); the spectrum is height-normalised to have the same integrated intensity as (*a*); (– – – –) simulation using $\delta B_L = 1.14$ mT, $\delta B_G^0 = 0.63$ mT. (*c*) X = S in 0.1 mol dm^{-3} $[NBu^n_4][ClO_4]$–dmf at *ca.* 100 K (2 mW, 0.16 mT, 9.133 GHz)

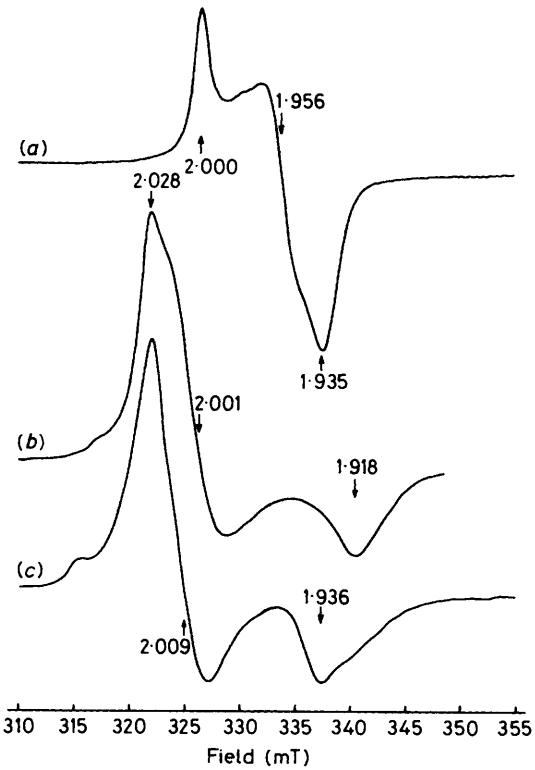

Figure 6. E.s.r. spectra for $[Fe_2X_2(XPh)_4]^{2-}$ (X = S or Se) reduced in dmf and frozen as a non-vitreous solid (microwave power 20 mW, microwave frequency 9.140 GHz). (*a*) Reduced $[Fe_2S_2(SePh)_4]^{2-}$ (field modulation amplitude 0.32 mT). (*b*) Reduced $[Fe_2Se_2(SPh)_4]^{2-}$ (0.5 mT). (*c*) Reduced $[Fe_2Se_2(SePh)_4]^{2-}$ (0.5 mT)

Reduction of $[Fe_2S_2\{(SCH_2)_2C_6H_4\text{-}o\}_2]^{2-}$ in 0.1 mol dm^{-3} $[NBu^n_4][ClO_4]$–dmf containing excess Bu^{t}SH was observed to give a very similar spectrum to that described above for the dimers with unidentate arenethiol ligands, Figure 4(*b*) (*g* extrema 2.020, 1.882, and 1.846). A similar sample prepared using $[Fe_2S_2\{(SCH_2)_2C_6H_4\text{-}o\}_2]^{2-}$ enriched to 83% in ^{57}Fe gave an e.s.r. spectrum which has its low-field peak split according to the expected statistical distribution of ^{57}Fe–^{56}Fe in a coupled dimer, Figure 4(*c*). Because the lines composing this peak are so narrow (half-height at half-width 0.43 mT) the splitting for ^{57}Fe–^{56}Fe (1 : 1) and ^{57}Fe–^{57}Fe (1 : 2 : 1) may be clearly seen. A simulation performed by field shifting the natural-abundance ^{56}Fe spectrum with the ^{57}Fe hyperfine splitting, and adding component spectra according to the expected statistical distribution for the three isotopic mixtures,[7] achieves a good fit to the experimental spectrum using an average splitting of 1.4 mT [Figure 4 (*c*)]. The same splitting was found in a similar analysis for $[Fe_2S_2\{(SCH_2)_2C_6H_4\text{-}o\}_2]^{3-}$ (ref. 7) and for the $[2Fe\text{–}2S]^+$ ferredoxins from *Pseudomonas putida* [14] and spinach.[15]

For $[Fe_2S_2(btpo)_2]^{2-}$ reduced in the presence of 50-fold excess Bu^{t}SH the same type of signal is found (*g* extrema at 2.020, 1.896, and 1.842 in 0.2 mol dm^{-3} $[NBu^n_4][ClO_4]$–mpo).

Reduction of selenium-substituted dimers. Spectra for reduced $[Fe_2X_2\{(SCH_2)_2C_6H_4\text{-}o\}_2]^{2-}$ (X = S or Se) in dmf are compared in Figure 5, demonstrating a shift to higher mean *g* value on going from sulphur bridging ($g_{average} = 1.956$) to selenium bridging (*g* extrema 2.030, 1.979, and 1.930; $g_{average} = 1.980$). A similar shift is seen for reduced $[Fe_2X_2(btpo)_2]^{2-}$ in dmf (X = S: $g_{average} = 1.951$. X = Se: $g_\perp = 2.051$, $g_\parallel = 1.947$, $g_{average} = 1.982$). Both the chelated selenium-bridged complexes, like their sulphur homologues, have signals with *g* values which are independent of the state of glassification of the frozen solvent. The low-field feature of the reduced-$[Fe_2Se_2(btpo)_2]^{2-}$ signal shows the same asymmetry apparent in the spectrum for the corresponding sulphur complex (Figure 3). In both sets of chelated complexes the spectra for the selenium-bridged dimer broaden in a lower temperature range than for the sulphur-bridged dimer.

E.s.r. spectra from reduction of selenium-substituted complexes which are co-ordinated by unidentate aryl chalcogenide ligands display solvent and vitrification dependence similar to that already described for reduced $[Fe_2S_2(SC_6H_4Y\text{-}p)_4]^{2-}$ complexes. Spectra of the corresponding type N from non-vitreous samples of $[Fe_2Se_2(SPh)_4]^{2-}$ and $[Fe_2S_2(SePh)_4]^{2-}$ reduced in dmf are shown in Figure 6 (*b*) and (*a*) and have sets of *g* extrema at 2.028, 2.001, and 1.918 and at 2.000, 1.956, and 1.935 respectively. Similar spectra may be obtained in mpo. Reduced $[Fe_2Se_2(SC_6H_4Me\text{-}p)_4]^{2-}$ shows a spectrum very similar to that of Figure 6(*b*). In the spectrum for $[Fe_2Se_2(SePh)_4]^{2-}$ reduced in dmf [Figure 6(*c*)] the major signal has *g* extrema at 2.028, 2.009, and 1.936, but significant contributions are seen from a peak at $g = 2.070$ and a shoulder at $g = 1.915$. These latter, together with other small additional features seen in the spectra of Figure 6 (*a*) and (*b*), may originate from signals characteristic of the glassy samples or else must be ascribed to impurities generated in the reduction.

Table 2. E.s.r. data for $[2Fe–2X]^+$ centres in reduced $[Fe_2X_2(XR)_4]^{2-}$ (X = S or Se) complexes and in ferredoxins

(*a*) Pre-reduced compound	Solvent [a]	Conditions	g_z	g_y	g_x	Ref. in Figure 8
$[Fe_2Se_2\{(SCH_2)_2C_6H_4\text{-}o\}_2]^{2-}$	dmf (nv)		2.030	1.979	1.930	h
$[Fe_2Se_2\{(SCH_2)_2C_6H_4\text{-}o\}_2]^{2-}$	dmf (v)	0.1 mol dm^{-3} $[NBu^n_4][ClO_4]$	2.032	1.981	1.928	i
$[Fe_2Se_2(btpo)_2]^{2-}$	dmf (v)	0.1 mol dm^{-3} $[NBu^n_4][ClO_4]$	2.051	1.947	1.947	b
$[Fe_2Se_2(SPh)_4]^{2-}$	dmf (nv)		2.028	2.001	1.918	k
$[Fe_2Se_2(SPh)_4]^{2-}$	mpo (nv)		2.030	2.004	1.917	
$[Fe_2S_2(SePh)_4]^{2-}$	dmf (nv)		2.000	1.956	1.935	d
$[Fe_2Se_2(SePh)_4]^{2-}$	dmf (nv)		2.028	2.009	1.936	j
$[Fe_2Se_2(SC_6H_4Me\text{-}p)_4]^{2-}$	dmf (nv)		2.030	1.999	1.914	
$[Fe_2Se_2(SPh)_4]^{2-}$	dmf (v)	0.2 mol dm^{-3} $[NBu^n_4][ClO_4]$	2.047	1.928	1.879	
$[Fe_2Se_2(SPh)_4]^{2-}$	dmf (v)	17% CH_2Cl_2	2.048	1.929	1.880	
$[Fe_2Se_2(SPh)_4]^{2-}$	mpo (v)	0.2 mol dm^{-3} $[NBu^n_4][ClO_4]$	2.033	1.882	1.837	
$[Fe_2S_2(SePh)_4]^{2-}$	mpo (v)	0.2 mol dm^{-3} $[NBu^n_4][ClO_4]$	2.019	1.908	1.824	

(*b*) Ferredoxins	Ref.	g_z	g_y	g_x	Ref. in Figure 8
Pig adrenal glands	23	2.043	1.967	1.953	(xiii)
Beef adrenal glands	23	2.051	1.975	1.959	(xiii)
Parsley	*b*	2.061	1.965	1.937	(xiv)
P. putida	23	2.042	1.980	1.943	(xv)
Beef adrenal glands (mixed S,Se)	23	2.038	1.973	1.934	(xvi)

[a] See footnote *a* of Table 1. [b] J. A. Fee and G. Palmer, *Biochim. Biophys. Acta*, 1971, **245**, 175.

Reductions of the selenium-substituted complexes in the presence of 0.1—0.2 mol dm^{-3} $[NBu^n_4][ClO_4]$ to give vitreous samples lead to solvent-dependent spectra. In each case these contain more features than can be straightforwardly analysed into sub-spectra, but g extrema of the major (> *ca.* 70%) contributing lineshapes are reported in Table 2 for selected samples.

Spin-Lattice Relaxation in the Reduced Dimers.—The temperature dependence of the spin-lattice relaxation times, T_1, of several $[2Fe–2S]^+$ ferredoxins in the region of broadening of their e.s.r. spectra has been interpreted in terms of dominant Orbach relaxation processes involving excited states at energies which may be related to the $S = \frac{3}{2}$ level of the spin manifold resulting from the antiferromagnetic coupling of the iron(II) and iron(III) ions.[16–19] A similar interpretation may be placed upon T_1 measurements for the $[Fe_2S_2\{(SCH_2)_2C_6H_4\text{-}o\}_2]^{3-}$ paramagnetic ion, indicating an exchange interaction $J = -300 \pm 15$ cm^{-1}.[20]

Values of T_1 have been determined for the e.s.r. signals from $[Fe_2Se_2\{(SCH_2)_2C_6H_4\text{-}o\}_2]^{2-}$ and $[Fe_2S_2(SC_6H_4Cl\text{-}p)_4]^{2-}$ reduced in dmf, Figures 5 (*a*) and (*b*) and 1 (*a*) respectively, by analysis of the temperature-dependent broadening of their low-field (B_z) peaks in the range *ca.* 90—200 K.

The method of deducing T_1 from the spectral broadening is based on that described by Bertrand *et al.*[21] A detailed account of the specific analytical procedure used here has been given for the e.s.r. spectra of $[Fe_2S_2\{(SCH_2)_2C_6H_4\text{-}o\}_2]^{3-}$ in various solvents,[20] and we confine the present description of this method to a brief outline.

Firstly, the B_z peak of the low-temperature spectrum was least-squares fitted with a convolution function between Lorentzian and Gaussian lineshapes, as depicted for the selenium-bridged dimer in Figure 5. In this procedure the simulation curve was accurately positioned over the experimental curve by superposition of the crossover points of their derivatives, and squared differences between the curves accumulated from the start of the spectrum to a point just above B_z. The higher temperature spectra were simulated in a similar manner with a convolution product between the same Gaussian function of constant half-width δB_G^0 and an increasingly broad Lorentz function of half-width δB_L. Additional temperature-dependent Lorentzian broadening, $\delta B_L'$, was calculated by subtraction of the residual low-temperature Lorentz component, δB_L^0, and related to the spin-lattice relaxation time [equations (1) and (2) (units in parentheses)].

$$\delta B_L' = \delta B_L - \delta B_L^0 \quad (1)$$

$$\frac{1}{T_1}(s^{-1}) = \frac{g\beta}{\hbar} \cdot \delta B_L' \text{ (mT)} \quad (2)$$

Reduced $[Fe_2Se_2\{(SCH_2)_2C_6H_4\text{-}o\}_2]^{2-}$. E.s.r. spectra of the reduced $[Fe_2Se_2\{(SCH_2)_2C_6H_4\text{-}o\}_2]^{2-}$ sample used in the T_1 measurements are shown in Figure 5 (*a*) and (*b*) at 86 and 161 K. A small isotropic impurity signal was observed in these spectra at $g = 2.003$, but was outside the field range of the lineshape analysis. At the lowest temperature the B_z peak could be analysed in terms of a Gaussian contribution having half-width at half-height $\delta B_G^0 = 0.63$ mT and a Lorentzian contribution with $\delta B_L^0 = 0.39$ mT. These values are similar to those ($\delta B_G^0 = 0.62$ mT and $\delta B_L^0 = 0.29$ mT) found for $[Fe_2S_2\{(SCH_2)_2C_6H_4\text{-}o\}_2]^{3-}$ in the same solvent, and could well have similar origins.[20] Significant broadening at B_z is apparent above *ca.* 110 K and could be successfully extracted up to *ca.* 170 K. Above this temperature the lineshapes were not so well formed due to depletion in intensity. Also, at the highest temperatures employed (*ca.* 190 K) some irreversible broadening occurred, probably due to crystalline structural changes in the solvent matrix.

The derived T_1 data are plotted in Figure 7 against temperature and the full data-points linear least squares fitted according to the relationship expected for a dominant Orbach relaxation mechanism, equation (3), with $\Delta = 600$ cm^{-1}

$$1/T_1 = A \cdot \exp(-\Delta/kT) \quad (3)$$

[standard error in $\Delta = 5$ cm^{-1}; $A = (2.9 \pm 0.2) \times 10^{10}$ s^{-1}; correlation coefficient = 0.992]. Although the standard error in Δ is less than 1%, an error of 5% is deemed more appro-

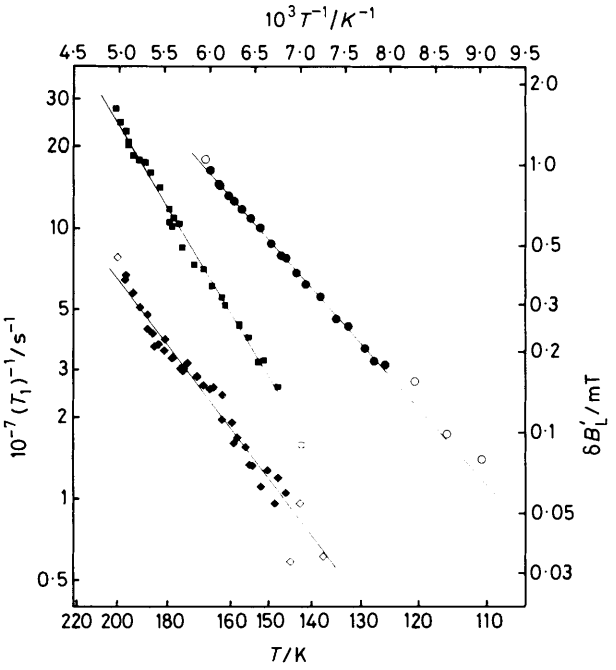

Figure 7. Temperature dependence of T_1 (from $\delta B_L'$) for $[Fe_2X_2\{(SCH_2)_2C_6H_4\text{-}o\}_2]^{3-}$ (X = S or Se) and $[Fe_2S_2(SC_6H_4Cl\text{-}p)_4]^{3-}$ in dmf; the data for the latter complex has been halved in value for purposes of clarity in the presentation. The lines, which correspond to equation (3) and the data given in the text, are a least-squares fit to the points marked by filled symbols. Data points marked with open symbols, at the extremes of the temperature range, were considered less reliable for reasons described in the text: $[Fe_2S_2(SC_6H_4Cl\text{-}p)_4]^{3-}$ (♦, ◇), Δ = 710; $[Fe_2S_2\{(SCH_2)_2C_6H_4\text{-}o\}_2]^{3-}$ (■, □), Δ = 900; $[Fe_2Se_2\{(SCH_2)_2C_6H_4\text{-}o\}_2]^{3-}$ (●, ○), Δ = 600 cm^{-1}

priate, as judged by making alternative acceptable fits to the data.

Reduced $[Fe_2S_2(SC_6H_4Cl\text{-}p)_4]^{2-}$. After reduction and transfer to the sample tube the solution of $[Fe_2S_2(SC_6H_4Cl\text{-}p)_4]^{2-}$ in dmf was frozen in an isopentane slush-bath rather than in liquid nitrogen, in order to produce a finely crystalline solvent lattice. In this way problems with lineshape changes at high temperatures due to solvent crystalline structural reorganisation could be mitigated and the contribution from the type W vitreous-solvent signal minimised. A small peak at g *ca.* 2.017 attributable to type W or VW signal was in fact still discernible in the spectra and necessitated the use of a weighting function such that the squared difference between the experimental and calculated peaks was not accumulated in this region, so as to avoid distorting the fit to the g = 2.002 peak.

The sample was studied at 85—200 K. At the lowest temperatures the B_z peak was found to be a product of a Gaussian function of half-height at half-width δB_G^0 = 0.44 mT with a residual Lorentzian function for which δB_L^0 = 0.63 mT. Little broadening was seen below 130 K. Extraction of the additional Lorentz broadening $\delta B_L'$ could be achieved with adequate accuracy between 150 and 190 K, and the corresponding T_1 data from two incremental temperature cycles are presented in Figure 7. (Note that the data values have been halved to clarify the overall presentation.) The data are reasonably well fitted with a line according to equation (3) with Δ = 710 ± 70 cm^{-1} [standard error in Δ = 20 cm^{-1}; coefficient A = (2.1 + 0.4) × 10^{10} s^{-1}; correlation coefficient = 0.9858].

Discussion

Reduction Products.—The observations made for the e.s.r. spectra obtained on reducing the complexes $[Fe_2S_2(SC_6H_4Y\text{-}p)_4]^{2-}$ (Y = Cl, H, or Me) under various conditions may be summarised as follows.

(1) On reduction in pure solvents which freeze to a non-vitreous state the main or only component in the e.s.r. spectra of all three complexes has very similar and nearly solvent-independent g values at 2.001—2.002, 1.952—1.958, and 1.911—1.915 (type N).

(2) Reduction in solvent mixtures which vitrify on freezing results in an increased proportion of a signal with solvent-dependent g values: 2.013—2.016, 1.908—1.913, and 1.870—1.874 in dmf (type W); 2.019—2.020, 1.894—1.895, and 1.817—1.824 in mpo (type VW).

(3) Formation of the type W and VW signals is promoted in the order Y = Cl < H < Me.

(4) A type W signal in a glassy dmf sample reversibly changes to a type VW signal on conversion of the sample to a non-vitreous state.

(5) Reduction in the presence of excess thiol ligand promotes formation of the type N signal.

(6) Bu^{t}SH and EtSH added before or after reduction in glass-forming solvent mixtures produces new signals having quite large anisotropy intermediate between that of the type W and VW signals (g = 2.019—2.021, 1.887—1.894, and 1.842—1.846).

In order to classify the various signals observed we use the theoretical interpretation of g tensor variations in [2Fe–2S]$^+$ ferredoxins developed by Bertrand and Gayda.[22,23] They consider a rhombic C_{2v} distortion in the ligand environment of the Fe^{2+} ion, having the same geometrical character for each protein, but variable in intensity. Differences in the g extrema amongst the reduced ferredoxins may then be correlated with the variable mixing of the two A_1 (C_{2v}) d-orbital states consequential upon the proposed distortional differences. Assuming some reasonable approximations, Bertrand and Gayda showed that g_x and g_y are functions solely of the d-orbital mixing, which for small distortions can be directly related to $(g_y - g_x)$. They showed the low-field g extremum, g_z, to be a function both of the orbital mixing and of the energy separation, Δ_{xy}, between the two lowest orbital states. The three g extrema for several ferredoxins, and also for some of the selenium-substituted homologues, are plotted in Figure 8 against $(g_y - g_x)$ in the manner of Bertrand and Gayda,[22,23] together with the theoretical curves of these authors, which show a good agreement with the experimental data. Also plotted in this figure are the g values found for the complexes $[Fe_2X_2(XR)_4]^{2-}$ [2XR = $(SCH_2)_2C_6H_4$-o or btpo; R = $-C_6H_4Y$-p (Y = Cl, H, or Me); X = S or Se] reduced in the various solvent systems. A clear distinction is demonstrated between the g values for the type N signals and also the $(SCH_2)_2C_6H_4$-o chelated complex in comparison with those for the type W and type VW spectra observed with vitreous samples. The former fit well with the experimental protein values and with the analysis of Bertrand and Gayda. For the type W and type VW signals, on the other hand, g_x and g_y depart considerably below values expected for [2Fe–2S]$^+$ ferredoxin centres. A comparable differentiation between the signal types is found using the analysis of g value variation in reduced ferredoxins presented by Blumberg and Peisach:[24] the g values typical of the type W and type VW spectra are found to lie at some considerable separation from the main [2Fe–2S]$^+$ ferredoxin trends which incorporate the type N signals.

The signal with g extrema at *ca.* 2.007, 1.940, and 1.922 observed on reduction of $[Fe_2S_2\{(SCH_2)_2C_6H_4\text{-}o\}_2]^{2-}$ in several solvent systems is considered to arise from the cor-

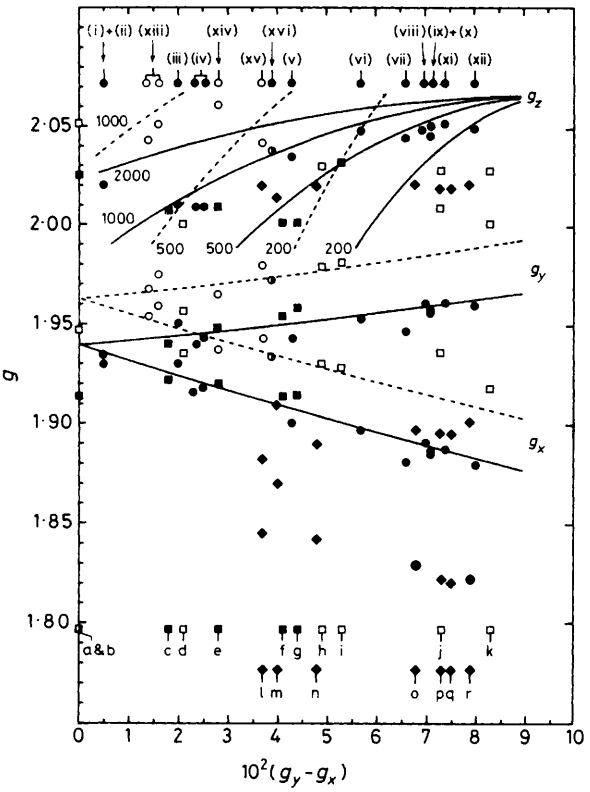

Figure 8. A plot of g extrema for 2Fe-ferredoxins and for spectra of the reduced model complexes against $10^2(g_y - g_x)$. Filled symbols correspond to the native ferredoxins and to complexes which are both bridged and terminally ligated by sulphur. Open symbols are for Se-substituted centres. Circular symbols are used for the proteins, square symbols for those complexes considered to result from one-electron reduction of precursor dianionic dimers, and diamond symbols for complexes where a chemical modification of the centre is believed to have occurred. The numbers (i)—(xvi) for the ferredoxins along the top and the letters for the model complexes along the bottom correlate firstly *via* their attached symbols to the data points and secondly to the numerical data of Tables 1 and 2. The full (S bridged) and dashed (Se bridged) lines are those derived by Bertrand and Gayda.[22,23] The numbers on the upper g_z curves are the Δ_{xy} splitting (cm^{-1})

responding trianion.[6,7] Although slightly different g values are found in mpo (Table 1) these are found also to be in good agreement with those of reduced ferredoxins and, similar to the type N signals from reduced $[Fe_2S_2(SC_6H_4Y\text{-}p)_4]^{2-}$ (Y = Cl, H, or Me), the spectra are not considered grossly dependent on the specific solvent employed.

On the basis of the compatibility of the type N signals with those for $[Fe_2S_2\{(SCH_2)_2C_6H_4\text{-}o\}_2]^{3-}$, and moreover, of the agreement of their g values with those for $[2Fe\text{–}2S]^+$ ferredoxins and the analysis of Bertrand and Gayda, the type N signals are attributed to the trianions $[Fe_2S_2(SC_6H_4Y\text{-}p)_4]^{3-}$ (Y = Cl, H, or Me) resulting directly from one-electron reduction of the corresponding dianionic starting materials. The other signals predominating in glassy samples, types W and VW together with the signals observed in the presence of excess Bu^{t}SH, are considered to arise from species having some chemical modification to the Fe_2S_6 core. We are at present unable to rationalise the diverse range of observations reported in the Experimental section in such a way as to determine the precise nature of the chemical modifications involved. We note, however, the following relevant points.

(*i*) The type W and VW signals most likely originate from dimeric chalcogenide-bridged species in view of the characteristic $g_{average} < 2.0$ and of their ready interconversion to type N signals attributable to $[Fe_2S_2(SR)_4]^{3-}$. In the cases of the type VW spectra in mpo and of the signals observed on reduction in the presence of excess Bu^{t}SH, Figure 4, the ^{57}Fe splitting further confirms a binuclear structure for the paramagnetic species.

(*ii*) As may be seen from Figure 8, selenium substitution for sulphur leads for any given symmetry to higher g values and this may be related to increased covalency at the Fe^{III} ion. The shift of the type W and type VW signals, characteristic of vitreous samples, to lower g values compared with their type N counterparts, may result from decreased covalency at the Fe^{III} ion, perhaps due to substitutional co-ordination by a nitrogen- or oxygen-donor ligand from the solvent.

(*iii*) The reduced tetrameric iron–sulphur clusters, $[Fe_4S_4(SR)_4]^{3-}$, are reported to have greatly increased reactivity compared with the corresponding dianions.[25–29] This gives precedent to the proposal of ligand substitution in the reduced dimer complexes which is not observed under the same conditions in the dianions; the latter, as monitored by visible spectrophotometry, were observed to be largely unaffected by any changes in the solvent system, including the addition of thiols such as Bu^{t}SH.

(*iv*) Promotion of the proportion of type N signal observed when reduction was carried out in the presence of excess ligand thiol could be understood in terms of displacing an equilibrium involving replacement and, it must be supposed, protonation of one or more thiol ligands on going from type N to W or VW spectral species.

(*v*) The ordering Y = Cl < H < Me found for ease of production of type W and VW signals on reducing $[Fe_2S_2(SC_6H_4Y\text{-}p)_4]^{2-}$ is that of expected and observed increasing pK_a for $p\text{-}YC_6H_4SH$ on the basis of the Y substituent Taft parameter.[30,31] For $[Fe_4S_4(SR)_4]^{2-}$ the ease with which co-ordinated thiolate (RS^-) is replaced by another ligand was found to increase with increasing pK_a of the thiol (RSH).[25,32,33] It is difficult to draw conclusions from the behaviour of $[Fe_2S_2\{(SCH_2)_2C_6H_4\text{-}o\}_2]^{3-}$ as although the ligand should, on account of its greater pK_a as an aliphatic thiolate, possess increased lability over the aromatic thiolates, this may be more than offset by enhanced chelation-incurred stability. Indeed, this ligand must be placed before $p\text{-}ClC_6H_4SH$ in the above series since no gross vitrification- or solvent-dependency is found in the e.s.r. spectrum on reduction of $[Fe_2S_2\{(SCH_2)_2C_6H_4\text{-}o\}_2]^{2-}$. The same lack of dependence on solvent or its state of vitrification is observed for the signals produced on reduction of $[Fe_2S_2(btpo)_2]^{2-}$ and this too may be understood in terms of superior stability inherent in the chelating btpo ligand compared to the unidentate thiolates.

These points would seem to indicate a reversible reaction in which on going from the species giving the type N signal to those giving the type W and VW signals, one or more thiol ligands, probably at the Fe^{III} ion, are reversibly displaced by another ligand, possibly solvent. There are, however, some difficulties with such an interpretation, for example with respect to point (*ii*), substitution by Bu$^tS^-$ or EtS^- would not be expected to lead to the gross decreases in mean g value which are observed when reductions are performed in excesses of the corresponding thiols. Another explanation of the latter behaviour then becomes necessary. With respect to point (*v*) and considering the solvents as potential ligands, their aprotic nature would preclude the involvement of a proton transfer to a thiolate ligand as the origin of a pK_a-dependent propensity to substitution.

The nature of the species giving the novel large anisotropy e.s.r. signals remains unresolved and will be the subject of future investigations. We note with interest, however, the

similarity between the type VW e.s.r. spectra having g extrema *ca.* 2.02, 1.895, and 1.82 and signals attributed to $[2Fe-2S]^+$ centres in certain enzymes. For the 4-methoxybenzoate *O*-demethylase from *P.putida* (putidamono-oxin) an e.s.r. signal has been reported with g values at 2.01, 1.91, and 1.78 [34] and for the oxidation factor of cytochrome b—c_1 in succinate–cytochrome c reductase a similar spectrum is observed with g values 2.02, 1.90, and 1.78.[35] The similarity of the signals for some of the synthetic dimer complexes in mpo to those for these proteins is of particular interest in that both proteins form part of enzyme complexes and may be directly involved in chemical modification processes during which additional or substitutional ligand co-ordination could take place.

For the type N signals the range of $(g_y - g_x)$ and their small overall resonance-field anisotropy is consistent with changes in $[2Fe-2S]^+$ ferredoxin spectra produced by solvents, chaotropic anions (material which slightly disrupts tertiary protein structure), or denaturing agents.[36–39] These agents cause a decrease of the large $(g_y - g_x)$ splitting found for plant ferredoxin signals. Of particular interest and relevance are the changes observed by Cammack *et al.*[36,37] when employing dmso or guanidine hydrochloride as denaturants. Under these conditions, where the protein is presumed unfolded so as to release any imposed strain and expose the core to the solvent, a variety of proteins produce similar spectra with g extrema in the range 2.0—1.9 similar to the type N signals attributed here to $[Fe_2S_2(SR)_4]^{3-}$ ions.

The spectra observed on reduction of $[Fe_2S_2(btpo)_2]^{2-}$, Figure 3, are somewhat anomalous. The analysis of Bertrand and Gayda [22] indicates that for an axial ferredoxin spectrum $g_\perp \simeq 1.94$, Figure 8, in contrast to the value of 1.914 for the spectrum in Figure 3(*a*). However, the spectra show solvent-independent behaviour which is comparable to that for $[Fe_2S_2\{(SCH_2)_2C_6H_4\text{-}o\}_2]^{3-}$ and for the type N signals attributable to $[Fe_2S_2(SC_6H_4Y\text{-}p)_4]^{3-}$, and it seems reasonable to assign the species responsible to $[Fe_2S_2(btpo)_2]^{3-}$. Deviation of the $g_\perp$ value from that expected in the theoretical treatment of Bertrand and Gayda could arise if any distortion at the Fe^{II} ion were not to comply to the C_{2v} symmetry which they assume. The btpo ligand is certainly likely to be the least flexible of those employed here and could well impose a strained co-ordination.

For the selenium-substituted dimers it seems reasonable, as with the sulphur homologues, to assign the signals for the $(SCH_2)_2C_6H_4$-*o* ligated dimer and for the non-vitreous samples containing aryl chalcogenide ligated dimers (Figures 5 and 6) to trianion species resulting directly from reduction of the dianions. Such a designation is made largely on the grounds of g value compatibility to the Bertrand–Gayda model (Figure 8) and because of their solvent-invariant lineshapes. The arguments outlined above for reduced $[Fe_2S_2(btpo)_2]^{2-}$ apply also to the selenium homologue, spectra for which [*e.g.* Figure 3(*c*)] are assigned to $[Fe_2Se_2(btpo)_2]^{3-}$.

The increased covalency upon substitution of two selenide bridging ligands for the sulphide results in higher Fe^{III} g values [40] and thus higher g values for the dimer.[23] This effect is amplified in reduced $[Fe_2Se_2(SePh)_4]^{2-}$ where the tetra-seleno-co-ordinated Fe^{III} ion is even more covalent,[40] so that the mean g value is observed to be closer to 2.0 than in the thiophenolate ligated homologue.

Relaxation Time (T_1) Measurements.—The T_1 data from temperature-dependent broadening at B_z in the e.s.r. spectra of $[Fe_2Se_2\{(SCH_2)_2C_6H_4\text{-}o\}_2]^{3-}$ and $[Fe_2S_2(SC_6H_4Cl\text{-}p)_4]^{3-}$, as presented in Figure 7, have been reasonably fitted according to a dominant Orbach relaxation mechanism. Also presented for comparison in Figure 7 is the variation with temperature of the spin-lattice relaxation time for $[Fe_2S_2\{(SCH_2)_2C_6H_4\text{-}o\}_2]^{3-}$ in dmf fitted according to an Orbach process involving an excited state at $\Delta \simeq 900$ cm^{-1}.[20] It was found that the T_1 data for this complex could also be not unreasonably fitted according to a $(1/T_1) \propto T^{7.5 \pm 0.3}$ relationship,[20] and in the same way it is possible to fit the data for $[Fe_2Se_2\{(SCH_2)_2C_6H_4\text{-}o\}_2]^{3-}$ to a $(1/T_1) \propto T^{6.0 \pm 0.2}$ process (correlation coefficient 0.999) and data for $[Fe_2S_2(SC_6H_4Cl\text{-}p)_4]^{3-}$ to $(1/T_1) \propto T^{6.0 \pm 0.4}$ (correlation coefficient 0.986). Temperature variation of T_1 according to such processes has, however, no readily plausible origin in this region. The exponent, n, in least-squares fits employing a $(1/T_1) \propto T^n$ process was found to be independent of solvent in the case of $[Fe_2S_2\{(SCH_2)_2C_6H_4\text{-}o\}_2]^{3-}$,[20] but changes from 7.5 to 6.0 on replacing sulphur-bridging ligands with selenium. For a non-resonant Raman relaxation mechanism the reverse behaviour might be anticipated since the relaxation process should be more dependent on the characteristics of the environment than the structure of the complex. For a dominant Orbach relaxation mechanism, however, the variation in slope of the linear fits shown in Figure 7 is clearly understood in terms of differences in the energies of the first excited state of the spin manifolds for the complexes, as determined by variation in the strength of the Fe^{III}–Fe^{II} exchange interaction. Dominance of an Orbach relaxation mechanism has been found applicable to interpretation of the T_1 temperature dependence in the regions of spectral broadening for a number of $[2Fe-2S]^+$ and $[4Fe-4S]^+$ ferredoxins [16–19,21,41–44] and the same mechanism, which is entirely compatible with the experimental findings (Figure 7), is reasonably expected of the $[2Fe-2S]^+$ model complexes studied in this work.

All these analyses in terms of two-phonon resonant relaxation mechanisms employ excited states having energies greater than the expected maximum available from phonons in the surrounding solvent or protein, and it is necessary to

Table 3. Antiferromagnetic coupling parameters, J, for $[2Fe-2X]^{(+,2+)}$ (X = S or Se) centres in ferredoxins and their synthetic analogues

Complex ion or protein source	$-J$/cm^{-1}	Ref.
(*a*) $[2Fe-2X]^+$		
$[Fe_2S_2\{(SCH_2)_2C_6H_4\text{-}o\}_2]^{3-}$	300 ± 15	7
$[Fe_2Se_2\{(SCH_2)_2C_6H_4\text{-}o\}_2]^{3-}$	200 ± 10	This work
$[Fe_2S_2(SC_6H_4Cl\text{-}p)_4]^{3-}$	240 ± 25	This work
Adrenodoxin (membrane)	270	18
Adrenodoxin (solution)	165 ± 10	17
Spinach [a]	110	*b*
Spinach	90 ± 5	17
Synechococcus lividus [a]	98 → 115	*c*
Spirulina maxima [a]	98^{+5}_{-10}	*d*
Spirulina maxima	83 ± 5	21
Scenedesmus	83	21
Halobacterium halobium	75 ± 5	17
Rieske centre	65	18
(*b*) $[2Fe-2S]^{2+}$		
$[Fe_2S_2\{(SCH_2)_2C_6H_4\text{-}o\}_2]^{2-}$ [a]	149 ± 8	3
Spirulina maxima [a]	182 ± 20	*d*

[a] Data from magnetic measurements; the remainder are from spin-lattice relaxation measurements. [b] G. Palmer, in 'Iron–Sulphur Proteins,' ed. W. Lovenberg, Academic Press, New York, 1973, vol. 2, ch. 8. [c] See footnote *l* of Table 1. [d] L. Petersson, R. Cammack, and K. K. Rao, *Biochim. Biophys. Acta*, 1980, **622**, 18.

invoke intermediate localised modes originating most likely in the solvent or ligand structure.[20,44,45]

The excited-state energies for $[Fe_2Se_2\{(SCH_2)_2C_6H_4\text{-}o\}_2]^{3-}$ and $[Fe_2S_2(SC_6H_4Cl\text{-}p)_4]^{3-}$ indicated by the Orbach interpretation are reasonable in magnitude for assignment to the $-3J$ splitting of the $S = \frac{3}{2}$ level from the doublet ground state, originating from the antiferromagnetic iron–iron interaction. Exchange parameters, $-J$, for these complexes are compared in Table 3 to values previously obtained for $[Fe_2S_2\{(SCH_2)_2C_6H_4\text{-}o\}_2]^{3-}$ and $[2Fe\text{–}2S]^{+}$ ferredoxins. An inverse relationship between $|J|$ and $(g_y - g_x)$ has been proposed for which rhombic distortion of the ligand field at the Fe^{II} ion leads to a large separation between g_y and g_x [22] and also to decreased exchange coupling due to reduced direct and indirect (bridging) Fe–Fe orbital overlap.[17,18] On this basis the decrease in the magnitude of the exchange interaction on going from $[Fe_2S_2\{(SCH_2)_2C_6H_4\text{-}o\}_2]^{3-}$ ($|J| = 300$ cm^{-1}) to $[Fe_2S_2(SC_6H_4Cl\text{-}p)_4]^{3-}$ ($|J| = 240$ cm^{-1}) is consistent with the increase in the $(g_y - g_x)$ separation from 0.018 to 0.044. Both $|J|$ values are, however, higher than would be anticipated from the empirical correlation with $(g_y - g_x)$ described for the $[2Fe\text{–}2S]^{+}$ ferredoxins,[17,18] and must reflect some difference between the proteins and the models. A preliminary study of the broadening of the e.s.r. spectrum for reduced $[Fe_2S_2(btpo)_2]^{2-}$ indicates a small $|J|$ value even though the g tensor is nearly axial. In this case the distortion at the Fe^{II} ion may, however, be rather different from that for the other reduced dimers and for ferredoxins as indicated by analysis of the g tensor. In addition, the overall lineshape for this complex (Figure 3) shows some peculiar complications compared with the other dimer spectra for which linewidth relaxation investigations have been made, manifest in the asymmetry of the low-field peak and hyper-Lorentzian shape in the ' wings ' together with a poor fit to the conventional simulation model.

Conclusions

E.s.r. spectroscopy proves to be a particularly useful technique in observing the reduced dimers in view of its selectivity for these species at liquid nitrogen temperatures, since precursor dianion and tetramer reaction products give no interfering signals. The peculiar solvent dependency of the spectra for the unidentate thiolate-ligated complexes, and the spectral changes in the presence of added thiol, seem indicative of a considerably enhanced reactivity compared with the dianionic dimers. In this respect, despite a considerable amount of data, it has not proved possible, with the present extent of investigation, to formulate an exact rationalisation for the origin of the various spectral differences observed using a variety of solvents and additives. Certainly the changes in the e.s.r spectra must result from some chemical modification of the co-ordination at one or both iron atoms, but the precise nature of the interactions between the dimer and solvent or added thiol have not been elucidated. Spectra assignable to $[Fe_2X_2(XR)_4]^{3-}$ (X = S or Se) species resulting from direct one-electron reduction may, however, be identified with some confidence, showing characteristics closely matching those of reduced ferredoxins.

In an attempt to reach a more complete understanding of the observations described here we are continuing in attempts better to stabilise the reduction products, and employing new thiolate ligands.

References

1 J. J. Mayerle, R. B. Frankel, R. H. Holm, J. A. Ibers, W. D. Phillips, and J. F. Weiher, *Proc. Natl. Acad. Sci. USA*, 1973, **70**, 2429.
2 J. J. Mayerle, S. E. Denmark, B. V. DePamphilis, J. A. Ibers, and R. H. Holm, *J. Am. Chem. Soc.*, 1975, **97**, 1032.
3 W. O. Gillum, R. B. Frankel, S. Foner, and R. H. Holm, *Inorg. Chem.*, 1976, **15**, 1095.
4 J. G. Reynolds and R. H. Holm, *Inorg. Chem.*, 1980, **19**, 3257.
5 B-K. Teo, R. G. Shulman, G. S. Brown, and A. E. Meixner, *J. Am. Chem. Soc.*, 1979, **101**, 5624.
6 P. K. Mascharak, G. C. Papaefthymiou, R. B. Frankel, and R. H. Holm, *J. Am. Chem. Soc.*, 1981, **103**, 6110.
7 P. Beardwood, J. F. Gibson, C. E. Johnson, and J. D. Rush, *J. Chem. Soc., Dalton Trans.*, 1982, 2015.
8 J. Cambray, R. W. Lane, A. G. Wedd, R. W. Johnson, and R. H. Holm, *Inorg. Chem.*, 1977, **16**, 2565.
9 R. W. Lane, J. A. Ibers, R. B. Frankel, and R. H. Holm, *Proc. Natl. Acad. Sci. USA*, 1975, **72**, 2868.
10 D. L. Klayman and T. S. Griffin, *J. Am. Chem. Soc.*, 1973, **95**, 197.
11 D. G. Foster, *Org. Synth. Coll. Vol.*, 1955, **3**, 771.
12 M. A. Bobrik, E. J. Laskowski, R. W. Johnson, W. O. Gillum, J. M. Berg, K. O. Hodgson, and R. H. Holm, *Inorg. Chem.*, 1978, **17**, 1402.
13 T. N. Sorrell and E. H. Cheesman. *Synth. Commun.*, 1981, **11**, 909.
14 J. C. M. Tsibris, R. L. Tsai, I. C. Gunsalus, W. H. Orme-Johnson, R. E. Hansen, and H. Bienert, *Proc. Natl. Acad. Sci. USA*, 1968, **59**, 959.
15 G. Palmer, *Biochem. Biophys. Res. Commun.*, 1967, **27**, 315.
16 J. P. Gayda, J. F. Gibson, R. Cammack, D. O. Hall, and R. Mullinger, *Biochim. Biophys. Acta*, 1976, **434**, 154.
17 J. P. Gayda, P. Bertrand, C. More, and R. Cammack, *Biochimie*, 1981, **63**, 847.
18 J. C. Salerno, T. Ohnishi, H. Blum, and J. S. Leigh, *Biochim. Biophys. Acta*, 1977, **494**, 191.
19 D. Sh. Burbaev and A. V. Lebanidze, *Biofizika*, 1979, **24**, 392.
20 P. Beardwood, J. F. Gibson, P. Bertrand, and J. P. Gayda, *Biochim. Biophys. Acta*, in the press.
21 P. Bertrand, G. Roger, and J. P. Gayda, *J. Magn. Reson.*, 1980, **40**, 539.
22 P. Bertrand and J. P. Gayda, *Biochim. Biophys. Acta*, 1979, **579**, 107.
23 P. Bertrand and J. P. Gayda, *Biochim. Biophys. Acta*, 1980, **625**, 337.
24 W. E. Blumberg and J. Peisach, *Arch. Biochem. Biophys.*, 1974, **162**, 502.
25 R. W. Johnson and R. H. Holm, *J. Am. Chem. Soc.*, 1978, **100**, 5338.
26 R. S. McMillan, J. Renaud, J. G. Reynolds, and R. H. Holm, *J. Bioinorg. Chem.*, 1979, **11**, 213.
27 B. A. Averill and W. H. Orme-Johnson, *J. Am. Chem. Soc.*, 1978, **100**, 5234.
28 G. Christou, R. V. Hageman, and R. H. Holm, *J. Am. Chem. Soc.*, 1980, **102**, 7600.
29 J. G. Reynolds and R. H. Holm, *Inorg. Chem.*, 1981, **20**, 1873.
30 L. P. Hammett, in ' Physical Organic Chemistry,' 2nd edn., McGraw-Hill, New York, 1970, p. 356.
31 J. P. Danehy and K. N. Parameswaran, *J. Chem. Eng. Data*, 1968, **13**, 386.
32 G. R. Dukes and R. H. Holm, *J. Am. Chem. Soc.*, 1975, **97**, 528.
33 L. Que, M. A. Bobrik, J. A. Ibers, and R. H. Holm, *J. Am. Chem. Soc.*, 1974, **96**, 4168.
34 F. H. Bernhardt, E. Heymann, and P. S. Traylor, *Eur. J. Biochem.*, 1978, **92**, 209.
35 B. L. Trumpower and C. A. Edwards, *FEBS Lett.*, 1979, **100**, 13.
36 R. Cammack, *Biochem. Soc. Trans.*, 1975, **3**, 482.
37 R. Cammack, K. K. Rao, and D. O. Hall, *Biochem. Biophys. Res. Commun.*, 1971, **44**, 8.
38 L. Kerscher, D. Oesterhelt, R. Cammack, and D. O. Hall, *Eur. J. Biochem.*, 1976, **71**, 101.
39 R. E. Coffman and B. W. Stavens, *Biochem. Biophys. Res. Commun.*, 1970, **41**, 163.
40 J. Schneider, B. Dischler, and A. Rauber, *J. Phys. Chem. Solids*, 1968, **29**, 451.

41 H. Blum, J. C. Salerno, R. C. Prince, J. S. Leigh, and T. Ohnishi, *Biophys. J.*, 1977, **20**, 23.
42 H. Blum, J. C. Salerno, and M. A. Cusanovich, *Biochem. Biophys. Res. Commun.*, 1978, **84**, 1125.
43 H. Blum, J. C. Salerno, P. R. Rich, and T. Ohnishi, *Biochem. Biophys. Acta*, 1979, **548**, 139.
44 J. P. Gayda, P. Bertrand, C. More, J. LeGall, and R. Cammack, *Biochem. Biophys. Res. Commun.*, 1981, **99**, 1265.
45 P. Bertrand, J. P. Gayda, and K. K. Rao, *J. Chem. Phys.*, 1982, **76**, 4715.

Received 27th August 1982; *Paper* 2/1493